Myosin light chain 3 serves as a receptor for nervous necrosis virus entry into host cells via the macropinocytosis pathway

Authors: Lan Yao[1,2,3†], Wanwan Zhang[1,2,3,†], Xiaogang Yang[1,2,3], Meisheng Yi[1,2,3*], Kuntong Jia[1,2,3*]

Affiliations:

[1]School of Marine Sciences, Sun Yat-sen University, Guangzhou 510000, China.

[2]Southern Marine Science and Engineering Guangdong Laboratory (Zhuhai), Zhuhai 519000, China.

[3]Guangdong Provincial Key Laboratory of Marine Resources and Coastal Engineering, Guangzhou 510000, China.

†These authors contributed equally to this work.

*Corresponding author. Email: jiakt3@mail.sysu.edu.cn; yimsh@mail.sysu.edu.cn

Abstract: *Nodaviridae* infections cause severe mortality in insects and fish, with nervous necrosis virus (NNV) posing significant threats to global fish populations. However, the host factors involved in NNV entry remain poorly understood. Here, we identify myosin light chain 3 from marine medaka (*Oryzias melastigma*) (MmMYL3) as a novel receptor for red-spotted grouper NNV (RGNNV), facilitating internalization via macropinocytosis. MmMYL3 directly binds the RGNNV capsid protein (CP), which dependents on the arm and S domains of CP and the EF-hand2 domain of MmMYL3. In vitro experiments showed that MmMYL3 siRNA, protein, anti-MYL3 antibodies or the arm domain synthetic peptides blocked RGNNV entry. Moreover, in vivo administration of MmMYL3 protein also inhibited RGNNV infection. Ectopic MmMYL3 expression enabled RGNNV internalization into resistant cells. Notably, MmMYL3 facilitated RGNNV internalization through the macropinocytosis pathway via the IGF1R-Rac1/Cdc42 axis. Collectively, our findings underscore MYL3's crucial role in NNV entry and its potential as an antiviral target.

One Sentence Summary: Myosin light chain 3 serves as a receptor for nervous necrosis virus entry into host cells via the macropinocytosis pathway through IGF1R-Rac1/Cdc42 signaling.

Keywords: *Nodaviridae*; nervous necrosis virus; myosin light chain 3; macropinocytosis; receptor

32 **INTRODUCTION**

33 Viral encephalopathy and retinopathy, also known as viral nervous necrosis, is a
34 highly contagious and pathogenic disease that infects more than 120 marine and freshwater
35 fish species, leading to mass mortalities and severe economic losses in the aquaculture
36 industry. The etiological agent responsible, nervous necrosis virus (NNV), belongs to the
37 *Nodaviridae* family, genus *Betanodavirus* and manifests as a nonenveloped single-stranded
38 RNA virus (*1*, *2*). The NNV genome is composed of two RNA segments: RNA1 encodes
39 the RNA-dependent RNA polymerase (RDRP), while RNA2 encodes the viral capsid
40 protein (CP), which plays a critical role in the initial interaction with host cell surface
41 receptors, thus facilitating viral entry (*3*, *4*).

42 Viral entry into host cells is a key determinant of host specificity, tissue tropism, and
43 viral pathogenicity, and involves intricate interactions between viral capsid proteins and
44 host cell receptors (*5*). Viruses utilize sophisticated strategies to attach to one or multiple
45 receptors, enabling them to cross the plasma membrane and access the necessary host cell
46 machinery (*6*). Viral receptors function not only as attachment moieties but also as entry
47 factors, coordinators of viral trafficking, and activators of signaling events (*7*). Therefore,
48 identifying virus receptors and understanding the mechanism of virus-receptor interaction
49 is critical for better preventing viral diseases. Although NNV exhibits a broad host tropism,
50 only heat shock cognate protein 70 (HSC70) , heat shock protein 90ab1 (HSP90ab1) and
51 Nectin1 have been identified as its receptor or co-receptor (*8–10*). Following NNV CP
52 protein recognizes the cellular surface receptor, the NNV enters the cell by receptor-
53 mediated endocytosis. Viruses usually take advantage of various endocytic pathways to
54 enter host cells, with clathrin-mediated endocytosis (CME), macropinocytosis, and

55 caveolar/raft-dependent endocytosis being the most extensively studied (*11*). Previous
56 studies revealed that NNV particles utilize the receptor-mediated CME and
57 macropinocytosis internalization pathways to invade host cells (*12*), with the former
58 facilitated by HSP90ab1 and HSC70 (*9*). However, the receptor responsible for mediating
59 NNV invasion of host cells through macropinocytosis remains unknown.

60 Among the diverse cellular factors that can serve as viral receptors, members of the
61 myosin family have emerged as intriguing candidates (*13*). The myosin family comprises
62 a wide range of actin-associated motor proteins that play a role in a variety of cellular
63 activities, including signal transduction, intracellular transport and cell division, etc. Up to
64 date, more than 40 known classes of myosin have been identified (*14*). Recent studies
65 underscore their significance in various viral infections. For instance, myosin heavy chain
66 9 has been identified as a crucial factor for various virus infection (*15*). Non-muscle myosin
67 heavy chain IIA serves as a functional entry receptor for herpes simplex virus-1 (*16*).
68 Additionally, myosin II light chain activation is essential for influenza A virus cell entry
69 through macropinocytosis (*17*).

70 Myosin light chain 3 (MYL3), a constituent of the myosin light chain family
71 predominantly found in muscle tissues, particularly the heart and skeletal muscles, plays a
72 pivotal role in muscle contraction by forming the myosin complex with myosin heavy chain
73 and facilitating actin filament sliding (*18*, *19*). Mutations in the MYL3 gene have been
74 associated with various muscle-related disorders, including cardiomyopathies and skeletal
75 muscle myopathies (*20*). However, the role of MYL3 in virus infection remains
76 undiscovered. Huang et al reported that *Epinephelus coioides* MYL3 might interact with

77 native NNV CP by proteomic analysis of immunoprecipitation (IP) assay (*21*), yet its
78 involvement in NNV infection, particularly its role in viral invasion, remains uncertain.
79 In this study, we unveil MYL3 of marine medaka (*Oryzias melastigma*) (MmMYL3)
80 as a novel NNV entry receptor, elucidating its facilitation of RGNNV entry into host cells
81 through macropinocytosis, mediated by the IGF1R-Rac1/Cdc42 pathway. These findings
82 offer novel insights into the intricate mechanisms underlying NNV entry and highlight
83 potential targets for the development of antiviral drugs.
84

85 **RESULTS**

86 **Interaction between MmMYL3 and CP**

87 First, a Co-IP assay was conducted to validate the interaction between MmMYL3 and
88 CP. MmMYL3 exhibited colocalization and co-precipitation with CP (Fig. 1, A and B).
89 GST-tag pull-down assays provided additional confirmation of the direct interaction
90 between MmMYL3 and CP, as well as MmMYL3 and RGNNV virions (Fig. 1, C and D).
91 SPR analysis further confirmed a direct interaction between MmMYL3 and CP, with
92 kinetics revealing association rate constant (Ka), dissociation rate constant (Kd), and
93 equilibrium dissociation constant (K_D) of 1.448×10^4 M^{-1} s^{-1}, 1.679×10^{-4} s^{-1}, and 2.95
94 μM, respectively (Fig. 1E). Additionally, the interaction between CP and MYL3 was
95 consistently observed in another marine fish species, *Lateolabrax japonicus* (Fig. 1F).
96 These results robustly affirm the binding affinity of MmMYL3 to CP.

97 **Domain mapping of the association between MmMYL3 and CP**

98 To delineate the domain of MmMYL3 required for interaction with CP, various Myc-
99 tagged distinct domains of MmMYL3 were constructed, and Co-IP assays revealed that

100 deletion of the EF-hand2 domain of MmMYL3 abolished its interaction with CP,
101 suggesting the essential role of the EF-hand2 domain (Fig. 2, A and B). Furthermore, to
102 ascertain which domain of CP is necessary for interaction with MmMYL3, we generated a
103 series of Myc-tagged CP deletion mutants (Fig. 2C). Co-IP assays revealed that deletion of
104 the arm domain and S domain of CP resulted the abrogation of its interaction with
105 MmMYL3 (Fig. 2D). Collectively, these findings indicate that MmMYL3 interacts with
106 the arm and S domain of CP through its EF-hand2 domain.

107 **Localization of MmMYL3 on the cell surface**

108 We next explored whether MmMYL3 is present on the cell surface, a prerequisite for
109 a functional viral receptor. Immunofluorescence (IF) assays in permeabilized and non-
110 permeabilized hMMES1 and HEK293T cells transfected with Myc-MmMYL3 revealed
111 MmMYL3 localization both at the cell surface and in the cytoplasm (Fig. 3, A and B).
112 Meanwhile, no immunofluorescent signal was detected on the surface of non-
113 permeabilized cells using anti-Actin abs. Conversely, in permeabilized cells treated with
114 Triton X-100, MmMYL3 proteins were found not only on the cell surface but in the
115 cytoplasm. To corroborate the cell surface localization of MmMYL3, a protease protection
116 assay was carried out. Besides, the addition of proteinase K resulted in the significant
117 reduction of MmMYL3 protein in nonpermeabilized HEK293T or hMMES1 cells
118 transfected with pCMV-Myc-MmMYL3 plasmid compared to the control without
119 proteinase K treatment (Fig. 3, C and D), confirmed that MmMYL3 is exposed on the
120 surface of these cells.

121 To visualize the colocalization of MmMYL3 with the cell membrane, PKH 26, a red
122 fluorescent dye that binds stably to the lipid region of the cell membrane, was used.
123 Colocalization of MmMYL3 with PKH 26 in hMMES1 cells was observed, further
124 corroborating its membrane association (Fig. 3 E). Flow cytometry analysis using Alexa
125 Fluor 488-conjugated anti-Myc antibody also indicated a proportional increase in
126 MmMYL3 surface expression with increasing MmMYL3 concentrations in HEK293T and
127 hMMES1 cells (Fig. 3F). Lastly, co-transfection of MmMYL3 with the membrane protein
128 Na+/K+-ATPase alpha 1 (ATP1A1) in HEK293T and hMMES1 cells showed clear
129 colocalization of MmMYL3 with ATP1A1 in both permeabilized and non-permeabilized
130 conditions (Fig. 3, G and H), further affirming the presence of MmMYL3 on the cell
131 surface. Collectively, these findings robustly demonstrate that MmMYL3 is localized on
132 the cell surface.

133 **MmMYL3 serves as a surface receptor of RGNNV**

134 To investigate whether MmMYL3 was involved in RGNNV infection, we first
135 examined the expression pattern of *MmMYL3* during RGNNV infection. *MmMYL3*
136 exhibited a significant highly expression from 2 to 48 hours post infection (hpi), peaking
137 at 4 hpi, indicating MmMYL3 might play a vital role in the early stages of RGNNV
138 infection (fig. S1). Ectopic expression of MmMYL3 significantly increased *CP* expression
139 and RGNNV titer (Fig. 4, A to C), while MmMYL3 knockdown resulted in decreased *CP*
140 gene transcription and virus titer (Fig. 4, D to F).

141 To further substantiate that MmMYL3 functions as a receptor for RGNNV infection,
142 commercial anti-human MYL3 abs and purified GST-tagged MmMYL3 proteins were

143 used to evaluate the role of MmMYL3 in the virus entry process. Notably, recombinant
144 MmMYL3 (fig. S2) proteins significantly reduced the entry of RGNNV into hMMES1
145 cells in a dose-dependent manner (Fig. 4, G and H) and treatment with anti-MYL3 abs (fig.
146 S3) resulted in a significant reduction in *CP* and *RDRP* levels at 2 and 4 hpi, suggesting
147 inhibition of RGNNV entry (Fig. 4, I and J). Moreover, synthetic peptides derived from
148 the arm domain of CP could block RGNNV entry in a dose-dependent manner (Fig. 4, K
149 and L).

150 Cellular receptors required for virus infection confer infectability when they are
151 expressed in an uninfectable cell type. To further demonstrate the receptor function of
152 MmMYL3, we tested whether overexpression of MmMYL3 could render typically
153 resistant cells susceptible to RGNNV infection. HEK293T cells, which are not naturally
154 permissive to RGNNV, were transfected with MmMYL3 or MmHSP90ab1 (a known NNV
155 receptor). First, we detected CP anti-reverse sequences (*CP (-)*), which is a replicative
156 intermediate for production of viral RNAs, in MmMYL3 or MmHSP90ab1-overexpressing
157 HEK293T cells post RGNNV infection, but not in empty vector transfected cells (Fig. 5A).
158 Similar with MmHSP90ab1, overexpression of MmMYL3 promoted the entry of RGNNV
159 into HEK293T cells (Fig. 5B). Additionally, like observations in hMMES1 cells, abundant
160 viral particles were observed in the cytoplasm of MmMYL3 overexpressing HEK293T
161 cells post RGNNV infection (Fig. 5C). The internalization of RGNNV into MmMYL3
162 overexpressing HEK293T cells was further evidenced by the intracellular
163 immunofluorescence localization of CP at 24 hpi (Fig. 5D). These results further support

164 the susceptibility conferred by MmMYL3 expression, highlighting its role as a receptor for
165 RGNNV.

166 **MmMYL3 is vital for RGNNV pathogenesis in marine medaka**

167 To evaluate the physiological relevance of MmMYL3 in RGNNV infection, marine
168 medaka were injected with mixtures of RGNNV and recombinant MmMYL3 protein or
169 GST control protein, respectively (Fig. 6A). Fish injected with the MmMYL3-RGNNV
170 mixture exhibited significantly higher survival rates compared to those injected with the
171 GST-RGNNV mixture (Fig. 6B), indicating a protective effect of MmMYL3 on viral
172 pathogenesis. Consistent with these findings, qRT-PCR analysis showed that CP
173 expression levels in the brain and eye tissues were markedly reduced in the medaka treated
174 with the MmMYL3 protein (Fig. 6C). Furthermore, histopathological analysis revealed
175 reduced pathological injury, in the eyes and brains of the fish treated with MmMYL3
176 protein, as evidenced by diminished vacuolization compared to the control group (Fig. 6,
177 D and E). These results strongly indicate that MmMYL3 plays a critical role in mediating
178 RGNNV infection and pathogenesis in marine medaka.

179 **Involvement of MmMYL3 in RGNNV Entry via Macropinocytosis**

180 Previous studies have reported macropinocytosis and CME as the primary routes of
181 NNV internalization. To determine whether macropinocytosis is involved in RGNNV
182 entry into hMMES1 cells, we used a panel of compounds to treat the cells prior to viral
183 infection, including EIPA (macropinocytosis inhibitor), Rottlerin (macropinocytosis
184 inhibitor), CPZ (CME inhibitor), and Nystatin (caveolin inhibitor). After treatment,

185 hMMES1 cells were infected with RGNNV, and viral copies in cell lysates were quantified
186 by qRT–PCR. The results indicated that EIPA, Rottlerin, and CPZ significantly inhibited
187 RGNNV infection compared with the dimethyl sulfoxide (DMSO) control (Fig. 7A),
188 whereas Nystatin had no obvious effect, indicating RGNNV enters hMMES1 cells via
189 macropinocytosis and CME pathways.

190 To clarify the role of MmMYL3 in the process of RGNNV endocytosis, MmMYL3-
191 overexpressing hMMES1 cells were treated with the previously mentioned inhibitors
192 before virus infection. qRT-PCR experiments demonstrated a significant, dose-dependent
193 reduction in internalized RGNNV with EIPA and Rottlerin treatments (Fig. 7B). Fluid-
194 phase uptake is a distinctive feature activated during macropinocytosis. Studies on various
195 viruses entering host cells via macropinocytosis have demonstrated a transient
196 enhancement in fluid-phase uptake (*22*). Dextran served as a macropinocytosis marker,
197 being taken up by cells during macropinocytosis. As expected, cells infected with RGNNV
198 displayed dextran-positive vesicles resembling larger, irregular macropinosomes at 4 hpi,
199 in contrast to mock-infected cells (Fig. 7C). Meanwhile, clusters of MmMYL3 were
200 observed co-localized with RGNNV CP protein in dextran-positive macropinosomes (Fig.
201 7D). These findings suggest that MmMYL3 facilitated RGNNV enter hMMES1 cells via
202 macropinocytosis.

203 **Involvement of MmIGF1R in MmMYL3-Mediated RGNNV Entry**

204 Macropinocytosis initiation necessitates the coordinated activation of multiple
205 signaling pathways, typically induced by growth factors that prompt the activation of
206 receptor tyrosine kinases (RTKs) (*23*). To determine whether RTK activation is essential

207 for RGNNV entry mediated by MmMYL3, a series of inhibitors of RTKs were utilized.
208 Inhibitors of IGF1R (AZD-3463, Picropodophyllin) could block MmMYL3-mediated
209 RGNNV entry, but inhibitors of InsR (NVP-TAE), EGFR (Gefitinib) and c-Met (SU11274)
210 had no significant effect on virus entry mediated by MmMYL3 (Fig. 8A). To further clarify
211 the relationship between MmMYL3 and MmIGF1R, MmMYL3-Myc and MmIGF1R-GFP
212 were co-transfected into HEK293T cells, and we found that MmMYL3 were colocalized
213 with MmIGF1R (Fig. 8B). Additionally, Co-IP assay showed that MmIGF1R could
214 interact with MmMYL3 through the extracellular domain (Fig. 8, C and D). Furthermore,
215 pull-down assay further validated the direct interaction between MmMYL3 and MmIGF1R
216 (Fig. 8E). Additionally, overexpression of MmIGF1R promoted the entry of RGNNV,
217 whereas knockdown of MmIGF1R by siRNA inhibited RGNNV entry (Fig. 8, F to I).
218 These results strongly indicate that MmIGF1R is tightly associated with MmMYL3-
219 mediated viral invasion.

220 **Rac1/Cdc42 contributes to RGNNV entry**

221 The Ras superfamily GTPases, particularly Rac1 and Cdc42, are essential regulators
222 of macropinocytosis, contributing to actin cytoskeletal reorganization and membrane
223 ruffling (*24*, *25*). We therefore examined the relationship between Rac1, Cdc42 and IGF1R.
224 Co-IP assays revealed the co-precipitation of MmRac1 and MmCdc42 with MmIGF1R
225 (Fig. 9, A and B). Furthermore, we found that MmRac1 and MmCdc42 could interact with
226 the intracellular region of MmIGF1R (Fig. 9, C and D). In addition, MmRac1 and
227 MmCdc42 were observed to co-localize with MmIGF1R (Fig. 9, E and F). To evaluate the
228 functional significance of MmRac1 and MmCdc42 in RGNNV internalization, hMMES1

229 cells were transfected with either MmRac1 or MmCdc42. Overexpression of either
230 MmRac1 or MmCdc42 enhanced RGNNV internalization, as demonstrated by increased
231 viral RNA levels (Fig. 9, G to J). In contrast, the specific inhibitors of Rac1 (EHT1864)
232 and Cdc42 (MLS-573151) significantly reduced RGNNV entry in a dose-dependent
233 manner (Fig. 9, K and L).

234 Actin filaments play a crucial role in facilitating membrane folding and vesicle
235 formation during macropinocytosis, thereby influencing the efficiency and regulation of
236 this cellular uptake mechanism. Thus, we further monitored actin rearrangement during
237 RGNNV infection in hMMES1 cells. hMMES1 cells were stained with DAPI and
238 iFluorTM-488 conjugated phalloidin at 4 hpi, specifically binding to the polymerized form
239 of actin (F-actin). Intriguingly, RGNNV infection led to depolymerization and changes in
240 actin distribution. The number of F-actin filaments decreased, and actin-driven membrane
241 protrusions co-localized with virions were observed on the cell surface of infected cells,
242 absent in mock-infected control cells (Fig. 9M). These results suggest that MmRac1 and
243 MmCdc42 facilitate RGNNV internalization by driving macropinocytosis through actin
244 cytoskeletal dynamics.

245

246 **Discussion**

247

248 NNV, an important fish virus, enters host cells by utilizing a range of host factors that
249 act as receptors and facilitate the process of endocytosis via an orchestrated mechanism.
250 Three host factors, HSP90ab1,HSC70 and Nectin1, have been identified as entry receptors
251 of NNV (*8–10*), however, disrupting their interaction with cells does only partially hinder

252 viral infection, suggesting that NNV likely utilizes additional, yet unidentified host
253 receptors or co-receptors. To establish infection, NNV utilized receptor-mediated
254 endocytosis to induce internalization of the virus/receptor complex, primarily including
255 CME and macropinocytosis (*12*). Although previous studies demonstrate that HSP90ab1
256 and HSC70 are responsible for NNV internalization via CME, the receptor and the
257 molecular mechanisms leading to NNV entry into cells via macropinocytosis remain to be
258 determined. In this study, we found that NNV gain entry into host cells via the interaction
259 between CP and its novel receptor MmMYL3. Subsequently, MmMYL3 engages with
260 IGF1R, leading to the activation of the Rac1/Cdc42 pathway, which induces actin
261 rearrangement and facilitates NNV macropinocytosis (Fig. 10).

262 Numerous data indicate the significance of myosin light chains in the functionality of
263 both cardiac and skeletal muscles. However, little is known about the function of myosin
264 light chains during virus infection (*26–28*). Here, we provide several lines of evidence
265 showing that MmMYL3 acts as a novel receptor of NNV. First, ectopic expression of
266 MmMYL3 facilitates internalization of RGNNV, which is mediated by the interaction
267 between the EF-hand2 domain of MmMYL3 and the arm and S domain of CP. Considering
268 that our previous study had reported that MmHSP90ab1, a known NNV receptor, interacted
269 with the linker region of CP (*9*). Thus, we speculated that NNV might have the ability to
270 utilize multiple receptors simultaneously for cell infection through these receptors binding
271 to the different domains of CP. Furthermore, interference with the MmMYL3 and CP
272 interaction with abs against MYL3, MmMYL3 fusion protein and CP arm domain peptides
273 significantly block NNV entry, providing a potential antiviral strategy against NNV

274 infection. In addition to these *in vitro* findings, our *in vivo* experiments further confirm the
275 physiological relevance of MmMYL3 in viral pathogenesis and highlight its potential as a
276 therapeutic target in aquaculture. More importantly, virus-resistant HEK293T cells are
277 rendered susceptible to RGNNV infection by overexpression of MmMYL3 alone. The
278 development of MmMYL3 overexpressing HEK293T cells model offers a valuable
279 platform for investigating viral infection mechanisms and conducting drug screening
280 studies. All these results suggested that MmMYL3 is a novel receptor that mediates NNV
281 entry. We also found that the interaction of MYL3 with CP was conserved across NNV
282 sensitive fish. Interestingly, NNV exhibits a broad species tropism, capable of infecting
283 diverse cell lines and various animal species examined thus far (*1*). This phenomenon may
284 be attributed in part to the robust conservation of MYL3. To the best of our knowledge,
285 this is the first study to provide evidence that MYL3 functions as a functional entry receptor
286 for virus.

287 *Nodaviridae* viruses are divided into two genera: *Alphanodavirus* and *Betanodavirus*.
288 *Alphanodaviruses* typically infect insects, whereas *Betanodaviruses* primarily infect fish
289 (*29*). In recent years, a novel *Alphanodavirus*, provisionally named covert mortality
290 nodavirus (CMNV), has emerged, causing viral covert mortality disease in shrimp and also
291 affecting farmed marine fish (*30*, *31*). Given the susceptibility of marine fish to CMNV,
292 we investigated the possibility that both *Alphanodavirus* and *Betanodavirus* utilize MYL3
293 as a common receptor for cellular entry. Sequence comparison results revealed a low
294 homology between the CP protein sequences of CMNV and RGNNV. Additionally, our
295 data indicated that the CP of CMNV did not interact with MmMYL3 (data not shown).

296 These findings suggest that MmMYL3 may function as a receptor specific to
297 *Betanodavirus*, rather than being a common receptor for both viral genera.

298 Previous reports have highlighted the dependence of the NNV entry process on both
299 CME and macropinocytosis pathways (*12*). We had demonstrated NNV can use
300 MmHSP90ab1 and MmHSC70 to enter cells via CME pathway (*8*, *9*). In contrast to these
301 receptors, our findings revealed that MmMYL3 promotes NNV internalization via
302 macropinocytosis. Macropinocytosis, characterized as a transient, growth factor-induced,
303 actin-dependent endocytic pathway, facilitates the internalization of fluid and membrane
304 into large vacuole (*32*). Mounting evidence underscores its pivotal role as an endocytic
305 route exploited by numerous viruses for invading host cell (*33–35*). Upon binding to the
306 cell membrane, viruses trigger the activation of RTKs or other signaling molecules such as
307 Rac1, Cdc42, and Pak1, initiating intricate intracellular signaling cascades that lead to
308 alterations in actin filament dynamics and induction of plasma membrane ruffling (*24*, *25*,
309 *36*). RTKs, well-known upstream regulatory factors of macropinocytosis, are involved in
310 the entry process of various viruses (*37*, *38*). To evaluate the significance of RTKs in NNV
311 entry, we conducted a screening of small molecules targeting the activation of specific
312 RTKs. Our findings revealed that AZD-3463 and Picropodophyllin, two inhibitors of
313 IGF1R, could impede MmMYL3-mediated RGNNV entry. IGF1R is a transmembrane
314 RTK involved in mediating cellular responses to IGFs and plays a significant role in
315 cellular processes such as growth, proliferation, and survival (*39*, *40*). Recent studies have
316 revealed an intriguing connection between IGF1R signaling and viral entry mechanisms,
317 particularly through macropinocytosis (*41*, *42*). Our findings revealed direct binding

318 between MmMYL3 and MmIGF1R, indicating that MmMYL3 might participated in the
319 macropinocytosis-mediated NNV entry through its interaction with MmIGF1R. Previous
320 study had identified IGF1R as an entry receptor for respiratory syncytial virus (*43*).
321 Consider the conservation of IGF1R, we investigated whether it could serve as a potential
322 receptor for NNV. However, our analysis indicated that MmIGF1R did not directly bind to
323 CP, indicating that MmIGF1R might not be the receptor for NNV.

324 To further explore how MmIGF1R promotes macropinocytosis and NNV
325 internalization, we investigate the effect of MmIGF1R downstream signaling on NNV
326 infection. IGF1R can activate GTPases, such as Cdc42 and Rac1, leading to rapid actin
327 reorganization and membrane ruffling, key processes in initiating macropinocytosis (*44*,
328 *45*). Increasing evidence has demonstrate that Cdc42 and Rac1 are essential for various
329 virus entry (*46–48*). We found that both MmRac1 and MmCdc42 interact with the
330 intracellular domain of MmIGF1R, and inhibition of MmRac1 and MmCdc42 significantly
331 impaired RGNNV entry. Conversely, overexpression of MmRac1 or MmCdc42 enhanced
332 NNV internalization. Actin filaments play a central role in driving the membrane dynamics
333 necessary for the formation and internalization of macropinosomes during
334 macropinocytosis. We found that there was a notable reorganization of F-actin filaments,
335 accompanied by the presence of actin-driven membrane protrusions that co-localized with
336 virions on the surface of RGNNV infected cells. All these results indicated that cytosis
337 MmIGF1R regulate Rac1/Cdc42 signaling to promotes macropinocytosis during NNV
338 infection. While previous studies have suggested that NNV enters host cells via

339 macropinocytosis, our study was the first to provide a detailed mechanism understanding
340 of this process.

341 Overall, MmMYL3 was identified as a novel functional receptor for RGNNV.
342 Moreover, MmMYL3 was involved in and facilitated RGNNV internalization through the
343 macropinocytosis pathway via the IGF1R-Rac1/Cdc42 axis. Our findings shed new light
344 on the molecular mechanism of RGNNV entry and provide a new perspective for the
345 development of antiviral therapies.

346 While our study provides strong evidence that MmMYL3 serves as a receptor for
347 RGNNV *in vitro*, one limitation of our research is the lack of *in vivo* experiments using
348 MmMYL3 knockout marine medaka. Conducting these knockout studies would further
349 validate the role of MmMYL3 in NNV infection in a whole organism context. Unlike well-
350 established model organisms like zebrafish or mice, gene editing in marine medaka is
351 fraught with difficulties, including technical complexity, precise embryo microinjection,
352 and the potential for off-target effects with CRISPR/Cas9 technology. The process is time-
353 consuming, requiring multiple breeding generations and thorough molecular screening to
354 establish homozygous knockout lines. Future research aimed at developing these knockout
355 models will greatly benefit from advances in gene editing technologies and standardized
356 protocols tailored to marine medaka.

357 **MATERIALS AND METHODS**

358 **Cell Culture**

359 hMMES1 cell line, derived from marine medaka embryo blastocysts, was demonstrated to
360 be susceptible to RGNNV. hMMES1 cells were cultivated in ESM4 medium at 28˚C as
361 previously described (9). HEK293T cells were cultured in DMEM medium supplemented
362 with 10% heat-inactivated fetal bovine serum (FBS, Yeasen, China) under standard
363 conditions of 37˚C with 5% CO_2.

364 **Virus generation**

365 The RGNNV strain, originally isolated from afflicted sea perch larvae and juveniles in
366 Guangdong Province, China, was propagated in LJB cells (*49*, *50*) and preserved as viral
367 stocks at −80˚C for use.

368 **Cell transfection and NNV infection**

369 hMMES1 in six-well plates (1×10^6 cells/well) were transfected with different
370 plasmids using Lipofectamine 8000 (Beyotime) following the manufacturer's instructions.
371 At 24 h post-transfection, the cells were infected with RGNNV at a multiplicity of infection
372 (MOI) of 1 for the indicated hours and examined by quantitative reverse transcription-PCR
373 (qRT-PCR).

374 To detect the viral titers, hMMES1 cells transfected with pCMV-Flag-MmMYL3 or
375 MmMYL3-siRNA were infected with RGNNV (MOI=1) at 28˚C for 4 h, the culture
376 medium was removed and incubated with fresh medium for 48 h, then the supernatant was
377 collected for viral titer assay as described previously (51).

378 **RNA interference**

379 Small interfering RNAs (siRNAs) targeting MmMYL3 (siMmMYL3) were
380 synthesized by the Ribobio company (Guangzhou, China), including siRNA-1 (5′-
381 GGCTCAACTTTGACGCCTT-3′), siRNA-2(5′-CTGAGCTGCGAATTGTGCT-3′),
382 siRNA-3 (5′-GCTGTAGCTTGCCTACAGA-3′), and control siRNA (NC) (5′-
383 UUCUCCGAACGUGUCACGUTT-3′). siRNAs targeting MmIGF1R (siMmIGF1R)
384 were siRNA-4 (5′-GCACAACTTGACAATCCGA-3′), siRNA-5 (5′-
385 CGTCACATCAAGTTATACA-3′), siRNA-6 (5′-GCAATCTGACGTACTACCT-3′).
386 Transfection of siRNAs was conducted using a mixture of three different siRNAs at
387 concentrations of 50 or 100 nM as described previously (*51*).

388 **qRT-PCR**

389 Total RNA of cultured cells was extracted with TRIzol reagent (Invitrogen, CA, USA)
390 according to the manufacturer's instructions and was further reverse transcribed into cDNA
391 through the GoScript^{TM} Reverse Transcription Mix (Promega, Madison, USA). A
392 LightCycler 480 II (Roche Applied Science, Germany) and qPCR SYBR Green Master
393 Mix (Yeasen) were used for qRT-PCR analysis by using gene-specific primers (Table S1).
394 mRNA relative expression levels were evaluated from triplicate experiments and
395 normalized to marine medaka *β-actin*. The relative fold induction of genes was calculated
396 using the threshold cycle ($2^{-\Delta\Delta CT}$) method and presented as mean ± standard deviation (SD).

397 **Western blot and Co-IP**

398 The cells were lysed with lysate buffer (Beyotime) and boiled for 10 min with 1%
399 SDS for SDS-PAGE separation. The proteins were transferred onto polyvinylidene

400 difluoride (PVDF) membranes (Millipore, USA) and then blocked with 5% nonfat dried
401 milk for 1 h at room temperature (RT), followed by incubation with primary antibodies at
402 4°C overnight, including anti-Flag (1:4,000), anti-Myc (1:4,000), anti-GFP (1:4,000), anti-
403 MYL3 (1:1,000) and anti-actin (1:4,000) antibodies. Subsequently, membranes were
404 further probed with goat anti-rabbit or anti-mouse IgG (H+L) highly cross-adsorbed
405 secondary antibodies (1:1,000) for 1 h at RT and analyzed using enhanced
406 chemiluminescence (ECL) immunoblotting detection reagents (Millipore, USA) on a
407 chemiluminescence instrument (Sage Creation, China).

408 For the Co-IP assay, cell extracts were incubated with anti-Flag/Myc/GFP magnetic
409 beads at 4°C overnight. After incubation, the beads were washed five times with lysis
410 buffer and eluted with 1% SDS buffer for boiling. The eluted samples were subjected to
411 Western blot analysis.

412 **Protein purification and pulldown assays**

413 The pET-GST-MmMYL3 and empty pET-GST were transformed into *Escherichia*
414 *coli* BL21 (DE3), separately. Bacteria were grown to an OD600 of 0.8–1.0 and then
415 induced with 0.5 mM IPTG for 12 h at 20°C in a shaking incubator. MYL3-GST protein
416 and GST protein were purified using the GST spin purification kit (Beyotime) according
417 to the manufacturer's instruction. Briefly, the bacterial solution was collected and washed
418 three times with PBS. Lysozyme was added to a final concentration of 1 mg/ml, and placed
419 on ice for 30 min, then centrifuged at 4°C for 10 min. The supernatant was purified using
420 the BeyoGold™ GST-tag Purification Resin as described previously (*52*). Finally, the

421 protein was eluted from the column. The purified protein was stained with Coomassie
422 brilliant blue.

423 GST-Tag magnetic beads were first mixed with the GST-fused MmMYL3s for 4 h at
424 RT. Then, the beads were incubated with protein lysates from HEK293T cells transfected
425 with pCMV-Flag-CP or p-EGFP-MmIGF1R at 4°C overnight and finally analyzed by
426 Western blotting. For the pulldown assay between MmMYL3 and RGNNV, the beads
427 incubated with GST-fused proteins were mixed with RGNNV viral stock (500 μL) at 4°C
428 for 4 h. Then, the beads were subjected to SDS-PAGE.

429 **Surface Plasmon Resonance (SPR) analysis**

430 Biacore™ T200 (GE, USA) was used to analyze the interaction between MmMYL3
431 and the CP protein. Briefly, purified CP protein was first diluted (20 μg/mL) with 200 μL
432 of sodium acetate buffer (10 mM, pH 4.0) and then flowed across the activated surface of
433 a CM5 sensor chip (BR100012, GE, USA) at a flow rate of 10 μL/min, reaching a
434 resonance unit (RU) of ~2 500. The remaining activated sites on the chip were blocked
435 with 75 μL of ethanolamine (1 M, pH 8.5). Serial concentrations of MmMYL3 protein (5,
436 10, 20, 40, 80 μM) in PBS buffer (0.01 M, pH 7.4) were applied to analyze their interactions
437 with immobilized CP at a flow rate of 10 μL/min. The K_D for binding and Ka and Kd rate
438 constants were determined using the BIA evaluation program (GE, USA).

439 **Proteinase K protection assay**

440 The proteinase K protection assay was performed as described previously with some
441 modification (*9*). Briefly, hMMES1 and HEK293T cells were seeded into 6-well culture

442 plates and transfected with pCMV-Flag-MmMYL3 plasmids for 24 h. After washed with
443 PBS for three times, one group of cells were treated with 10 μg/ml of proteinase K for 30
444 min in an ice water bath, another group was added with the same volume of PBS, the
445 reaction was stopped by addition of PMSF. Cells were then lysed with lysis buffer on ice
446 for 30 min, the whole cell lysates were resuspended in SDS loading buffer and analyzed
447 by Western blot using anti-Flag or anti-Actin abs.

448 **Flow cytometry**

449 Cells were seeded on six-well plates overnight and scraped off the plate and washed
450 with PBS. For detection of surface expression of MmMYL3, cells were suspended with
451 200 μL PBS and incubated with anti-Alexa Flour 488-Myc antibody at 2 μg/mL on ice for
452 2 h. Cells were then washed with PBS and analyzed by flow cytometry.

453 **Transmission electron microscopy (TEM)**

454 Cell samples and ultrathin sections for TEM were prepared as described previously
455 (*53*). Cells were collected and fixed at 4˚C for 24 h with 2.5% glutaraldehyde in 0.1 M PBS
456 (pH 7.4) and 2.0% osmium tetroxide in 0.1 M PBS in turn, ultrathin sections were observed
457 under a Philips CM10 transmission electron microscope.

458 **Immunofluorescence assays**

459 To examine the localization of MmMYL3 proteins on cells, IF assays were performed
460 as described previously with some modification (*54*). Briefly, hMMES1 and HEK293T
461 cells were seeded into 24-well culture plates on glass coverslips and were separately
462 transfected with pCMV-Myc and pCMV-Myc-MmMYL3 plasmids, respectively. After

463 transfection for 24 h, cells were washed with PBS, fixed with 4% paraformaldehyde for 10
464 min at RT. One group was treated with 0.2% Triton X-100 for membrane permeabilization,
465 and the other was not. After being washed three times with PBS, cells were blocked with
466 PBS containing 5% bovine serum albumin at RT for 1 h and then reacted with anti-Myc
467 abs (1:400) at 4˚C overnight. Anti-Actin abs were used as negative control. After three
468 times wash with PBS, cells were incubated with Alexa Fluor 555 goat anti-mouse IgG
469 (Invitrogen) at a dilution of 1:400 for 1 h at RT. Cells were then washed with PBS and
470 stained the cell nuclei with DAPI for 10 min. The coverslips were washed with PBS and
471 observed under an SP8 Leica laser confocal microscopy imaging system (SP8, Leica,
472 Germany).

473 For assessment of the colocalization, HEK293T cells plated on coverslips in 24-well
474 plates were transfected with different plasmids. After transfection for 24 h, cells were
475 washed with PBS then fixed and permeabilized as described above. The cells were
476 incubated with primary antibodies at 4°C overnight, including anti-Flag (1:400) and anti-
477 Myc (1:400) antibodies, followed by incubation with Alexa Fluor 555- or 488-conjugated
478 secondary antibodies against mouse or rabbit IgG (1:400). Finally, cells were observed
479 under a confocal microscope.

480 For cell membrane staining, hMMES1 cells were labeled with PKH 26 (red
481 fluorescent, MCE). PKH 26 was dissolved in DMSO to obtain 1 mM stock solution of
482 PKH 26. The stock solution was diluted with PBS at 1:100 to obtain the 10 μM working
483 solution. hMMES1 cells were incubated with the working solution at 28°C for 30 min.

484 After the incubation, the cells were washed using PBS to remove unlabeled cells and
485 detected as described above.

486 For RGNNV entry detection, HEK293T were transfected with pCMV-Flag-
487 MmMYL3 for 24h, and then infected with RGNNV (MOI=5). After infection for 24 h, the
488 cells were detected with IF assays, cells were incubated with rabbit anti-CP abs and
489 detected as described above.

490 To observe actin cytoskeleton dynamics after virus infection, hMMES1 cells were
491 exposed to RGNNV (MOI=1) at 4°C and incubated for 4 h. The temperature shift was
492 performed after washing with PBS by using prewarmed (28°C) serum-free medium for 30
493 min. Afterwards, cells were fixed with 4% paraformaldehyde and permeabilized with 0.2%
494 Triton X-100 at room temperature. The cells were incubated with anti-CP antibody (1:200)
495 at 4°C overnight. iFluorTM 488 phalloidin and DAPI were used to stain actin filaments
496 and nuclei of cells, respectively(*22*).

497 **Dextran uptake assay for macropinocytosis**

498 Following a published procedure (*23*), hMMES1 cells on cover slips were treated with
499 indicated chemical compound. After treatment, the cells were serum-starved for 16 h. The
500 cells were infected with RGNNV (MOI=1) in media containing Alexa Fluor 647-
501 conjugated dextran (10,000 MW), incubated for 4 h at 28˚C, and washed and fixed for 16
502 h with 4% PFA at 4˚C. For co-localization experiments, the cells also were stained for
503 MmMYL3 and CP using specific antibodies as described above. Samples were viewed and
504 evaluated by confocal microscopy.

505 **Blocking assays**

506 MYL3-GST protein was affinity-purified as described above. RGNNV (10^3 $TCID_{50}$)
507 were incubated with different concentrations (100 or 500 ng) of recombinant MYL3-GST
508 protein for 4 h at 4˚C. Then, hMMES1 cells were incubated with virus and protein mixtures
509 for 4 h at 4˚C. Similarly, cells were treated with 10^3 $TCID_{50}$ of RGNNV preincubated with
510 BSA (500 ng) as a control. Then, cells were harvested, CP and RDRP mRNA were
511 measured as described above.

512 hMMES1 cells were pre-seeded in 12-well plates overnight. Due to the unavailability
513 of anti-MmMYL3 abs and the high homogeneity of MYL3 at the N-terminus domain
514 between human and fish, cells were incubated with anti-human MYL3 abs (1:50) (Abcam)
515 for 4 h at 28˚C. After washed with fresh media, cells were infected with RGNNV (MOI=1)
516 at 4˚C for 2 and 4 h, respectively. As a control, hMMES1 cells were in parallel pretreated
517 with normal rabbit IgG. Cells were then washed three times with PBS to remove free virus
518 particles and harvested for total RNA extraction and qRT-PCR detection of RGNNV CP
519 and RDRP.

520 To evaluate the implication of arm (short peptide of CP, RTDAPVSKASTVTGFGRG,
521 Sangon, Shanghai) on RGNNV entry, hMMES1 cells were pretreated with different doses
522 (0, 5, 10, 20, 40 μM) of these samples for 4 h. Then, the virus (MOI=1) was subsequently
523 added to allow infection for 4 h. The virus-protein mixture was removed, and cells were
524 further cultured with fresh protein-containing medium for 24 h. The qRT-PCR protocols
525 were performed as described above.

526 **Inhibitor treatment assay**

527 Cells were treated with various inhibitors to investigate the endocytosis pathway
528 utilized by RGNNV for cell entry. hMMES1 cells or MmMYL3-overexpressing hMMES1
529 cells were treated with different inhibitors for 4 h, then infected with RGNNV (MOI=1)
530 for 4 h at 28˚C. Next, the cells were washed with PBS for three times to remove any
531 unbound viruses. DMSO was used as control. Total RNA of cells was extracted for qRT-
532 PCR detection.

533 **RGNNV infection of marine medaka**

534 Marine medaka were divided into two groups: the MmMYL3 group and the GST
535 group (n = 30 per group). Correspondingly, RGNNV (100 $TCID_{50}$) was incubated with
536 purified GST-tagged MmMYL3 recombinant protein or GST protein for 4 h at 4˚C, then
537 the mixtures were injected into two groups of marine medaka separately. The negative
538 control group of fishes were injected with the same volume of PBS. The survival rate of
539 each group was recorded every day by counting the numbers of dead fish. The log-rank
540 test method was used to analyze the differences between groups. Marine medaka were
541 necropsied and the eyes and brains were collected at day 5 post infection for further
542 measurement of viral loads and pathological analysis. **, $P < 0.01$. The animal study was
543 reviewed and approved by the Ethics Committee of Sun Yat-Sen University (Approval No.
544 SYSU-IACUC-2023-000168).

545 **Quantification and statistical analysis**

546 Data were collected from three independent experiments, analyzed with SPSS version
547 20.0, and presented as the means ± SDs. Student's *t* test or one-way analysis of variance
548 (ANOVA) was used for the statistical comparisons between two groups or multiple groups,
549 respectively. *P* value <0.05 was considered to indicate a statistically significant difference;
550 *P* value < 0.01 was considered to indicate a highly significant difference.

551 **Supplementary Materials**

552 Materials and Methods

553 Fig.S1. Expression analysis of MmMYL3 in hMMES1 cells at 2, 4, 24 and 48 h post
554 RGNNV infection.

555 Fig.S2. Recombinant expression and purification of MmMYL3-GST and GST.

556 Fig.S3. MYL3 antibody validation.

557 Table S1. Primer sequences used by application.

558 **References and Notes:**

559 1. B. L. Munday, J. Kwang, N. Moody, Review article Betanodavirus infections of
560 teleost ® sh : a review. *J. Fish Dis.*, 127–142 (2002).

561 2. J. Z. Costa, K. D. Thompson, Understanding the interaction between Betanodavirus
562 and its host for the development of prophylactic measures for viral encephalopathy
563 and retinopathy. *Fish Shellfish Immunol.* **53**, 35–49 (2016).

564 3. I. Bandín, S. Souto, Betanodavirus and VER Disease: A 30-year. *Pathogens* **9**, 1–
565 46 (2020).

566 4. K. I. Mori, T. Nakai, K. Muroga, M. Arimoto, K. Mushiake, I. Furusawa, Properties
567 of a new virus belonging to nodaviridae found in larval striped jack (Pseudocaranx
568 dentex) with nervous necrosis. *Virology* **187**, 368–371 (1992).

569 5. J. Grove, M. Marsh, The cell biology of receptor-mediated virus entry. *J. Cell Biol.*
570 **195**, 1071–1082 (2011).

571 6. Melissa S. Maginnis, Virus-Receptor Interactions:The Key to Cellular Invasion. *J.*
572 *Mol. Biol.* **430**, 2590–2611 (2018).

573 7. M. Marsh, A. Helenius, Virus entry: Open sesame. *Cell* **124**, 729–740 (2006).

574 8. J.-S. Chang, S.-C. Chi, GHSC70 Is Involved in the Cellular Entry of Nervous
575 Necrosis Virus. *J. Virol.* **89**, 61–70 (2015).

576 9. W. Zhang, K. Jia, P. Jia, Y. Xiang, X. Lu, W. Liu, M. Yi, Marine medaka heat shock
577 protein 90ab1 is a receptor for red-spotted grouper nervous necrosis virus and
578 promotes virus internalization through clathrin-mediated endocytosis. *PLoS Pathog.*
579 **16**, 1–21 (2020).

580 10. Z. Zhang, J. Xing, X. Tang, X. Sheng, H. Chi, W. Zhan, Nectin1 is a pivotal host
581 factor involved in attachment and entry of red-spotted grouper nervous necrosis
582 virus in the early stages of the viral life cycle. *J. Virol*. (2024).

583 11. J. Mercer, M. Schelhaas, A. Helenius, Virus entry by endocytosis. *Annu. Rev.*
584 *Biochem.* **79**, 803–833 (2010).

585 12. W. Liu, C. H. Hsu, Y. R. Hong, S. C. Wu, C. H. Wang, Y. M. Wu, C. Ben Chao, C.
586 S. Lin, Early endocytosis pathways in SSN-1 cells infected by dragon grouper
587 nervous necrosis virus. *J. Gen. Virol.* **86**, 2553–2561 (2005).

588 13. J. He, Y. Qiu, L. Tan, D. Duan, X. Yuan, L. Yang, A. Wang, Understanding the key
589 functions of Myosins in viral infection. *Biochem. Soc. Trans.* **50**, 597–607 (2022).

590 14. B. J. Foth, M. C. Goedecke, D. Soldati, New insights into myosin evolution and
591 classification. *Proc. Natl. Acad. Sci. U. S. A.* **103**, 3681–3686 (2006).

592 15. L. Li, B. Xue, W. Sun, G. Gu, G. Hou, L. Zhang, C. Wu, Q. Zhao, Y. Zhang, G.
593 Zhang, J. A. Hiscox, Y. Nan, E. M. Zhou, Recombinant MYH9 protein C-terminal
594 domain blocks porcine reproductive and respiratory syndrome virus internalization
595 by direct interaction with viral glycoprotein 5. *Antiviral Res.* **156**, 10–20 (2018).

596 16. J. Arii, H. Goto, T. Suenaga, M. Oyama, H. Kozuka-Hata, T. Imai, A. Minowa, H.
597 Akashi, H. Arase, Y. Kawaoka, Y. Kawaguchi, Non-muscle myosin IIA is a
598 functional entry receptor for herpes simplex virus-1. *Nature* **467**, 859–862 (2010).

599 17. I. Banerjee, Y. Miyake, S. Philip Nobs, C. Schneider, P. Horvath, M. Kopf, P.
600 Matthias, A. Helenius, Y. Yamauchi, Influenza A virus uses the aggresome
601 processing machinery for host cell entry. *Science (80-.).* **346**, 473–477 (2014).

602 18. J. Ingles, A. Doolan, C. Chiu, J. Seidman, C. Seidman, C. Semsarian, Compound
603 and double mutations in patients with hypertrophic cardiomyopathy: implications
604 for genetic testing and counselling. *J. Med. Genet.* **42**, 2–7 (2005).

605 19. C. Zhang, J. Wang, G. Wang, Z. Ji, L. Hou, Z. Liu, T. Chao, Molecular cloning and
606 mRNA expression analysis of sheep MYL3 and MYL4 genes. *Gene* **577**, 209–214
607 (2016).

608 20. A. Mavilakandy, H. Ahamed, Mutation of the MYL3 gene in a patient with mid-
609 ventricular obstructive hypertrophic cardiomyopathy. *BMJ Case Rep.* **15**, 1–5
610 (2022).

611 21. P. Y. Huang, H. C. Hsiao, S. W. Wang, S. F. Lo, M. W. Lu, L. L. Chen, Screening
612 for the Proteins That Can Interact with Grouper Nervous Necrosis Virus Capsid
613 Protein. *Viruses* **12**, 1–20 (2020).

614 22. S. Delpeut, G. Sisson, K. M. Black, C. D. Richardson, Measles Virus Enters Breast
615 and Colon Cancer Cell Lines through a PVRL4-Mediated Macropinocytosis
616 Pathway. *J. Virol.* **91** (2017).

617 23. Y. Y. Zhang, R. Liang, S. J. Wang, Z. W. Ye, T. Y. Wang, M. Chen, J. Liu, L. Na,
618 Y. L. Yang, Y. B. Yang, S. Yuan, X. Yin, X. H. Cai, Y. D. Tang, SARS-CoV-2
619 hijacks macropinocytosis to facilitate its entry and promote viral spike–mediated
620 cell-to-cell fusion. *J. Biol. Chem.* **298**, 102511 (2022).

621 24. D. Bar-Sagi, F. McCormick, R. J. Milley, J. R. Feramisco, Inhibition of cell surface
622 ruffling and fluid-phase pinocytosis by microinjection of anti-ras antibodies into
623 living cells. *J. Cell. Physiol.* **133**, 69–73 (1987).

624 25. D. Bar-Sagi, J. R. Feramisco, Induction of membrane ruffling and fluid-phase
625 pinocytosis in quiescent fibroblasts by ras proteins. *Science (80-.).* **233**, 1061–1068
626 (1986).

627 26. K. E. Kamm, J. T. Stull, Signaling to myosin regulatory light chain in sarcomeres.
628 *J. Biol. Chem.* **286**, 9941–9947 (2011).

629 27. H. Yu, S. Chakravorty, W. Song, M. A. Ferenczi, Phosphorylation of the regulatory
630 light chain of myosin in striated muscle: methodological perspectives. *Eur. Biophys.*
631 *J.* **45**, 779–805 (2016).

632 28. F. Sheikh, R. C. Lyon, J. Chen, L. Jolla, HHS Public Access. **569**, 14–20 (2016).

633 29. C. Y. Yong, S. K. Yeap, A. R. Omar, W. S. Tan, Advances in the study of nodavirus.
634 *PeerJ* **2017**, 1–31 (2017).

635 30. Q. Zhang, Q. Liu, S. Liu, H. Yang, S. Liu, L. Zhu, B. Yang, J. Jin, L. Ding, X. Wang,
636 Y. Liang, Q. Wang, J. Huang, A new nodavirus is associated with covert mortality
637 disease of shrimp. *J. Gen. Virol.* **95**, 2700–2709 (2014).

638 31. C. Wang, S. Liu, K. F. J. Tang, Q. Zhang, Natural infection of covert mortality
639 nodavirus affects Zebrafish (Danio rerio). *J. Fish Dis.* **44**, 1315–1324 (2021).

640 32. J. Mercer, A. Helenius, Virus entry by macropinocytosis. *Nat. Cell Biol.* **11**, 510–
641 520 (2009).

642 33. J. K. Locker, A. Kuehn, S. Schleich, G. Rutter, H. Hohenberg, R. Wepf, G. Griffiths,
643 Entry of the two infectious forms of vaccinia virus at the plasma membane is

signaling-dependent for the IMV but not the EEV. *Mol. Biol. Cell* **11**, 2497–2511 (2000).

34. J. Mercer, A. Helenius, Vaccinia virus uses macropinocytosis and apoptotic mimicry to enter host cells. *Science (80-.).* **320**, 531–535 (2008).

35. C.-Y. Huang, T.-Y. Lu, C.-H. Bair, Y.-S. Chang, J.-K. Jwo, W. Chang, A Novel Cellular Protein, VPEF, Facilitates Vaccinia Virus Penetration into HeLa Cells through Fluid Phase Endocytosis. *J. Virol.* **82**, 7988–7999 (2008).

36. A. P. L. A. S. & P. P. D. F. Letizia Lanzetti, Rab5 is a signalling GTPases. *Nature* **429**, 309–314 (2004).

37. A. V. Nicola, J. Hou, E. O. Major, S. E. Straus, Herpes Simplex Virus Type 1 Enters Human Epidermal Keratinocytes, but Not Neurons, via a pH-Dependent Endocytic Pathway. *J. Virol.* **79**, 7609–7616 (2005).

38. M. Amyere, B. Payrastre, U. Krause, P. Van Der Smissen, A. Veithen, P. J. Courtoy, Constitutive macropinocytosis in oncogene-transformed fibroblasts depends on sequential permanent activation of phosphoinositide 3-kinase and phospholipase C. *Mol. Biol. Cell* **11**, 3453–3467 (2000).

39. M. Pellegrino, V. Secli, S. D'Amico, L. L. Petrilli, M. Caforio, V. Folgiero, N. Tumino, P. Vacca, M. Vinci, D. Fruci, E. de Billy, Manipulating the tumor immune microenvironment to improve cancer immunotherapy: IGF1R, a promising target. *Front. Immunol.* **15**, 1–10 (2024).

664 40. F. Hakuno, S. I. Takahashi, 40 years of IGF1: IGF1 receptor signaling pathways. *J.*
665 *Mol. Endocrinol.* **61**, T69–T86 (2018).

666 41. C. M. Stewart, A. Phan, Y. Bo, N. D. LeBlond, T. K. T. Smith, G. Laroche, P. M.
667 Giguère, M. D. Fullerton, M. Pelchat, D. Kobasa, M. Côté, Ebola virus triggers
668 receptor tyrosine kinase-dependent signaling to promote the delivery of viral
669 particles to entry-conducive intracellular compartments. *PLoS Pathog.* **17** (2021).

670 42. A. Józefiak, M. Larska, M. Pomorska-Mól, J. J. Ruszkowski, The igf-1 signaling
671 pathway in viral infections. *Viruses* **13**, 1–11 (2021).

672 43. C. D. Griffiths, L. M. Bilawchuk, J. E. McDonough, K. C. Jamieson, F. Elawar, Y.
673 Cen, W. Duan, C. Lin, H. Song, J. L. Casanova, S. Ogg, L. D. Jensen, B. Thienpont,
674 A. Kumar, T. C. Hobman, D. Proud, T. J. Moraes, D. J. Marchant, IGF1R is an entry
675 receptor for respiratory syncytial virus. *Nature* **583**, 615–619 (2020).

676 44. M. C. Manara, M. Terracciano, C. Mancarella, M. Sciandra, C. Guerzoni, M. Pasello,
677 A. Grilli, N. Zini, P. Picci, M. P. Colombo, A. Morrione, K. Scotlandi, CD99
678 triggering induces methuosis of Ewing sarcoma cells through IGF-1R/RAS/Rac1
679 signaling. *Oncotarget* **7**, 79925–79942 (2016).

680 45. D. H. M. Dam, X. Q. Wang, S. Sheu, M. Vijay, D. Shipp, L. Miller, A. S. Paller,
681 Ganglioside GM3 Mediates Glucose-Induced Suppression of IGF-1 Receptor–Rac1
682 Activation to Inhibit Keratinocyte Motility. *J. Invest. Dermatol.* **137**, 440–448
683 (2017).

684 46. T. Swaine, M. T. Dittmar, CDC42 Use in viral cell entry processes by RNA viruses.
685 *Viruses* **7**, 6526–6536 (2015).

686 47. F. Zhang, Y. Liu, Q. You, E. Yang, B. Liu, H. Wang, S. Xu, W. Nawaz, D. Chen,
687 Z. Wu, NSC23766 and Ehop016 suppress herpes simplex virus-1 replication by
688 inhibiting Rac1 activity. *Biol. Pharm. Bull.* **44**, 1263–1271 (2021).

689 48. Z. Z. Lu, C. Sun, X. Zhang, Y. Peng, Y. Wang, Y. Zeng, N. Zhu, Y. Yuan, M. S.
690 Zeng, Neuropilin 1 is an entry receptor for KSHV infection of mesenchymal stem
691 cell through TGFBR1/2-mediated macropinocytosis. *Sci. Adv.* **9**, 1–17 (2023).

692 49. P. Jia, K. T. Jia, M. S. Yi, Complete genome sequence of a fish nervous necrosis
693 virus isolated from sea perch (*Lateolabrax japonicus*) in China. *Genome Announc.*
694 **3**, 455643 (2015).

695 50. Y. Le, Y. Li, Y. Jin, P. Jia, K. Jia, M. Yi, Establishment and characterization of a
696 brain cell line from sea perch, Lateolabrax japonicus. *Vitr. Cell. Dev. Biol. - Anim.*
697 **53**, 834–840 (2017).

698 51. W. Zhang, J. Weng, L. Yao, P. Jia, M. Yi, K. Jia, Nectin4 antagonises type I
699 interferon production by targeting TRAF3 for autophagic degradation and
700 disrupting TRAF3-TBK1 complex formation. *Int. J. Biol. Macromol.* **218**, 654–664
701 (2022).

702 52. W. Lv, W. Jiang, H. Luo, Q. Tong, X. Niu, X. Liu, Y. Miao, J. Wang, Y. Guo, J. Li,
703 X. Zhan, Y. Hou, Y. Peng, J. Wang, S. Zhao, Z. Xu, B. Zuo, Long noncoding RNA
704 lncMREF promotes myogenic differentiation and muscle regeneration by

705 interacting with the Smarca5/p300 complex. *Nucleic Acids Res.* **50**, 10733–10755
706 (2022).

707 53. S. Dong, M. Kang, X. Wu, T. Ye, Development of a promising fish model (*Oryzias*
708 *melastigma*) for assessing multiple responses to stresses in the marine environment.
709 *Biomed Res. Int.* **2014** (2014).

710 54. K.-T. Jia, Y.-Y. Wu, Z.-Y. Liu, S. Mi, Y.-W. Zheng, J. He, S.-P. Weng, S. C. Li, J.-
711 G. He, C.-J. Guo, Mandarin Fish Caveolin 1 Interaction with Major Capsid Protein
712 of Infectious Spleen and Kidney Necrosis Virus and Its Role in Early Stages of
713 Infection. *J. Virol.* **87**, 3027–3038 (2013).

714 **Funding:**This work was supported by the National Natural Science Foundation of China
715 (32173001), Natural Science Foundation of Guangxi Province (2021GXNSFDA075015),
716 Scientific and Technological Planning Project of Guangzhou City (2023B03J1267),
717 Natural Science Foundation of Guangdong Province (2023B1515120074;
718 2024A1515010880) and Open Project Program of State Key Laboratory of Biocontrol
719 (2023SKLBC-KF03).

720 **Author contributions:** Conceptualization: M.Y and K.J.; Methodology: L.Y., W.Z. and
721 X.Y.; Investigation: L.Y. and W.Z.; Supervision: K.J., and M.Y; Funding acquisition: K.J.,
722 and M.Y; Writing – Original Draft: L.Y., W.Z., K.J., and M.Y.
723
724 **Competing interests:** The authors declare no competing interest.
725
726 **Data and materials availability:** All data are available in the main text or the
727 supplementary materials.

728 **Figure Legends:**

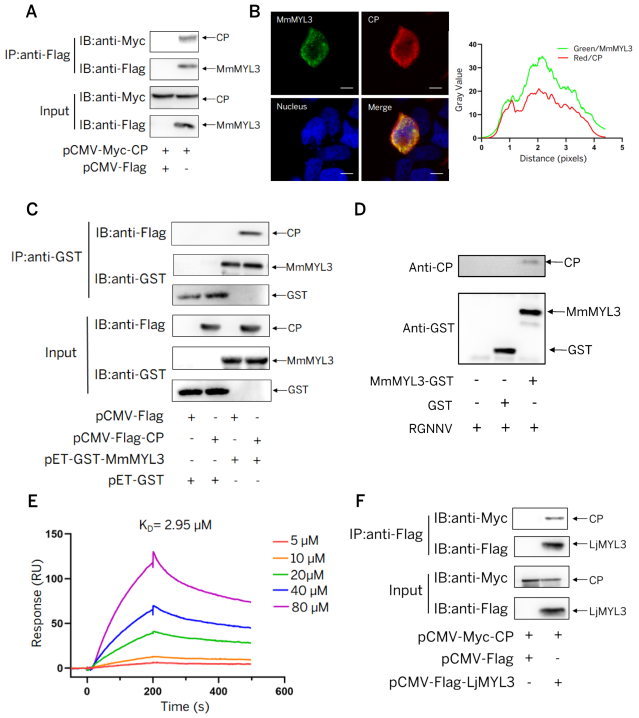

729
730 **Fig. 1. MmMYL3 interacts with CP.** (A) Immunoprecipitation (IP) (with anti-Flag) and
731 immunoblot analysis (with anti-Flag and anti-Myc) of HEK293 cells transfected with
732 plasmids encoding MmMYL3-Flag and CP-Myc for 48 h. (B) HEK293T cells were
733 cotransfected with MmMYL3-Flag and CP-Myc plasmids. MmMYL3 (green) and CP
734 (red) were detected by immunofluorescence staining with anti-Flag or anti-Myc abs,
735 respectively. Nucleus were stained by DAPI, Bar = 10 μm. (C) The lysates of HEK293T
736 cells transfected with indicated plasmids were pulled down with purified MmMYL3-GST
737 or GST proteins followed by immunoblotting with anti-GST and anti-Flag abs. (D) Pull-
738 down of RGNNV virions by MmMYL3-GST or GST proteins. RGNNV, purified proteins
739 and magnetic streptavidin beads were co-incubated as indicated. Pull-down was performed
740 with a magnet and the pellet was subjected to Western blot analysis. (E) SPR analysis of
741 MmMYL3-CP protein interaction. 1:1 binding model was used to calculate the K_D. (F)

742 Plasmids carrying MYL3 from sea perch (LjMYL3) were transfected into HEK293T cells,
743 together with CP-Myc plasmid. At 48 h posttransfection, the cell lysates were subjected to
744 coimmunoprecipitation analysis with anti-Flag magnetic beads as indicated.

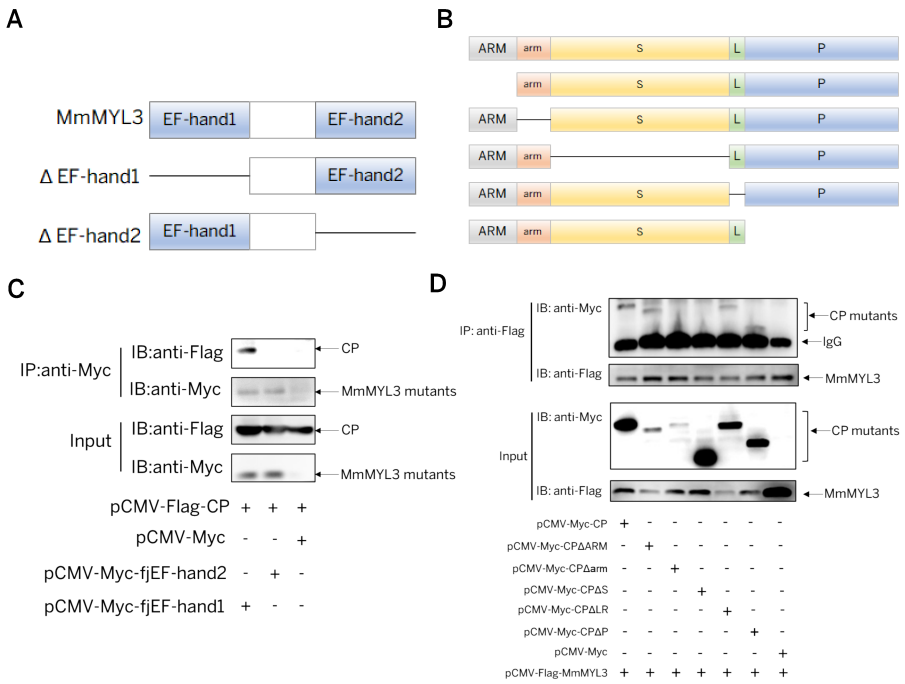

745

746 **Fig. 2. MmMYL3 interacts with the arm and S domains of CP through its EF-hand2**
747 **domain.** (A) Schematic diagram of MmMYL3 and its truncated mutants. (B)
748 Immunoprecipitation (IP) (with anti-Myc) and immunoblot analysis (with anti-Flag and
749 anti-Myc) of HEK293 cells transfected with plasmids encoding CP-Flag and Myc-tagged
750 full-length MmMYL3 or its truncated mutants for 48 h. (C) Schematic diagram of CP and
751 its truncated mutants. (D) HEK293T cells were cotransfected with MmMYL3-Flag and

752 different Myc-tagged CP mutants for 48 h. Co-IP assays were performed as described

753 above.

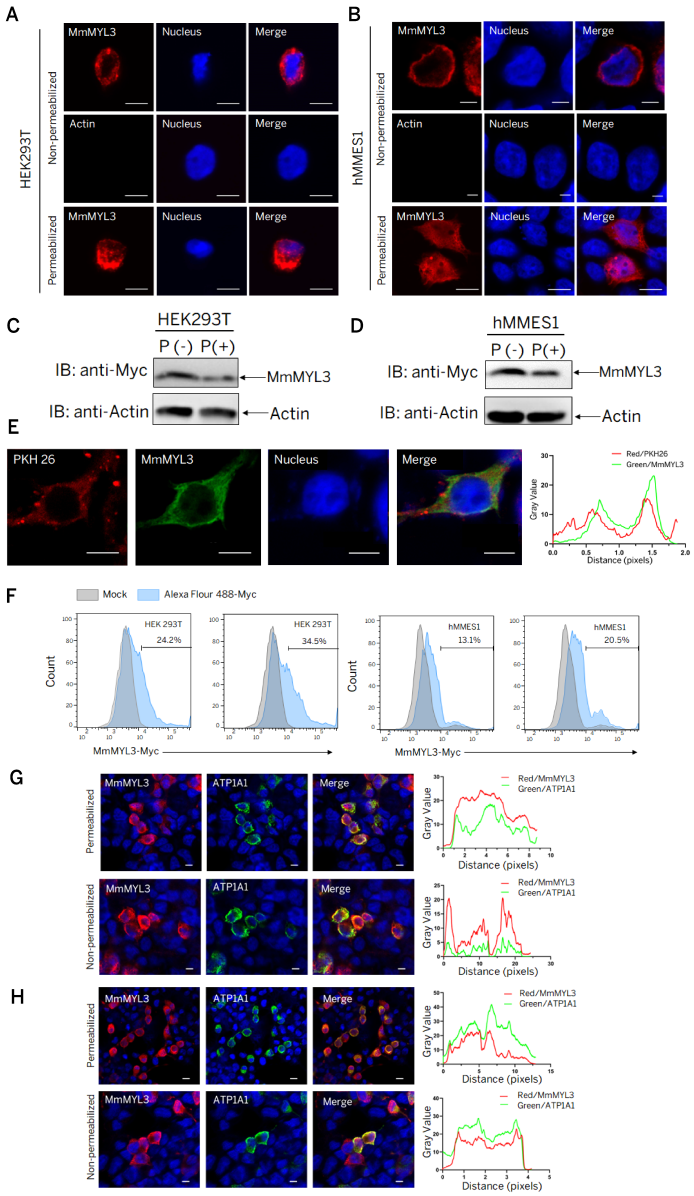

754

755 **Fig. 3. Surface localization of MmMYL3 in HEK293T and hMMES1 cells.** (A and B)

756 HEK293T (A) or hMMES1 (B) cells transfected with MmMYL3-Myc plasmids were fixed

757 with formalin, treated with Triton X-100 or not and immunostained with anti-Myc abs or

758 anti-Actin abs, respectively. Cell nuclei were stained with DAPI. Bar = 10 μm. (C and D)

759 HEK293T and hMMES1 cells transfected with MmMYL3-Myc plasmid were treated with
760 proteinase K (P+) or without proteinase K (P-) and harvested for a Western blot analysis
761 using anti-Myc and anti-Actin abs. (E) hMMES1 cells transfected with MmMYL3-Myc
762 plasmid were labeled with PKH 26 (red) and stained with anti-Myc abs (green). Nucleus
763 were stained by DAPI, Bar = 10 μm. (F) HEK293T and hMMES1 cells transfected with
764 Myc-MmMYL3 were stained with Alexa Fluor 488-conjugated anti-Myc abs. Surface
765 expression of MmMYL3 was analyzed by flow cytometry. (G and H) HEK293T or
766 hMMES1 cells were cotransfected with MmMYL3-Myc and ATP1A1-Flag plasmids.
767 MmMYL3 (red) and ATP1A1 (green) were detected by immunofluorescence staining with

768 anti-Myc or anti-Flag abs in permeabilized or non-permeabilized conditions. Nucleus were

769 stained by DAPI, Bar = 10 μm.

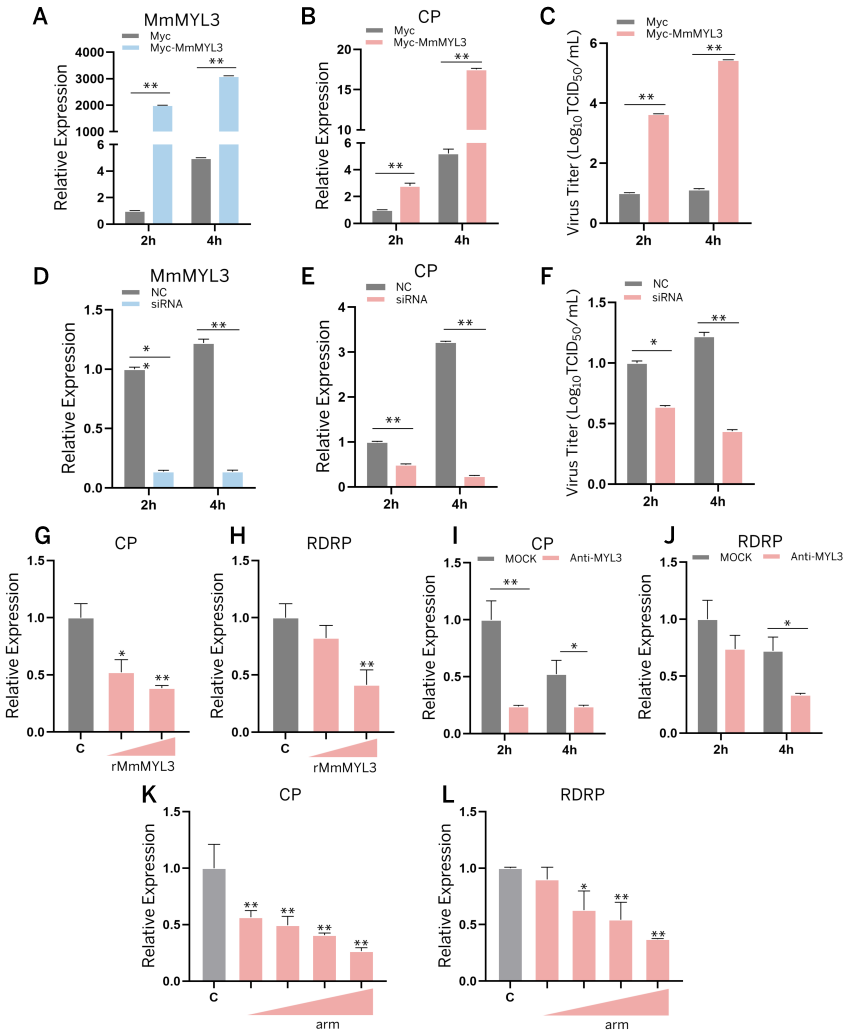

770

771 **Fig. 4. Effect of MmMYL3 on RGNNV entry.** (A and B) hMMES1 cells were transfected

772 with MmMYL3-Myc or Myc plasmid (Control) and infected with RGNNV (MOI = 1) for

773 2 and 4 h, respectively. Then, the cells were lysed for qRT-PCR to detect the expression of

774 MmMYL3 and CP. (C) Virus titer detection in MmMYL3-Myc transfected hMMES1 cells

775 post RGNNV infection for 2 and 4 h. (D and E) qRT-PCR analysis of MmMYL3 and CP

776 expression in siMmMYL3- or control-transfected hMMES1 cells infected with RGNNV

777 for 2 and 4 h. (F) Virus titer detection in siMmMYL3 transfected hMMES1 cells post
778 RGNNV infection for 2 and 4 h. (G and H) RGNNV was incubated with purified
779 MmMYL3-GST proteins (100 or 500 ng) for 4 h at 4˚C, then was added to hMMES1 cells
780 which were further incubated for 4 h at 4˚C. Cells were washed with PBS for three times
781 and harvested for CP (G) and RDRP (H) expression detection. (I and J) hMMES1 cells
782 were incubated with commercial anti-human MYL3 abs (1:50) for 4 h and then infected
783 with RGNNV for 2 or 4 h at 4˚C. After washed with PBS for three times, cells were
784 harvested for CP (I) and RDRP (J) expression detection. (K and L) hMMES1 cells were
785 treated with different concentrations of arm peptides for 2 h at 4˚C, and after RGNNV
786 infection for 4 h, CP (K) and RDRP (L) expression were detected by qRT-PCR. The results
787 are presented as mean ± SD. Statistical significance was determined by an unpaired two-

788 tailed Student's t test. *$P < 0.05$, **$P < 0.01$. Data are representative of three independent

789 experiments.

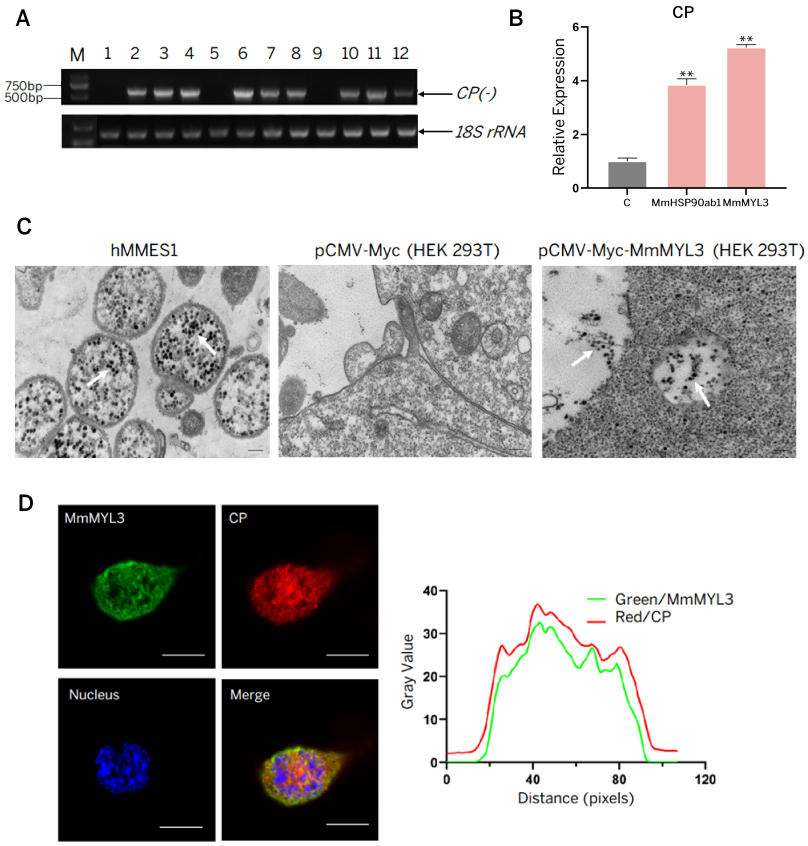

790

791 **Fig. 5. MmMYL3 was involved in RGNNV internalization**. (A) RT-PCR analysis of CP

792 (-) sequence. HEK293T cells were transfected with Myc empty vector (lines 1, 5, and 9),

793 MmMYL3-Myc (lines 2, 6, and 10), MmHSP90ab1-Myc (lines 3, 7 and 11), or both

794 MmMYL3-Myc and MmHSP90ab1-Myc (lines 4, 8, and 12) plasmids for 24 h,

795 respectively. Then cells were infected with RGNNV (MOI = 5) for 4 h. Next, the cells were

796 washed to remove any unbound viruses and incubated for 24 h (lines 1–4), 48 h (lines 5–

797 8) and 72 h (lines 9–12). Cells were harvested and total RNA was extracted for CP (-)

798 detection by RT-PCR. Human 18S rRNA was detected as a reference. (B) HEK293T cells

799 were transfected with MmMYL3-Myc, MmHSP90ab1-Myc or Myc plasmids,
800 respectively. Then, transfected cells were infected with RGNNV (MOI = 5) for 24 h. Next,
801 the cells were washed to remove any unbound viruses and total RNA was extracted for CP
802 detection by qRT-PCR. (C) Transmission electron micrograph of RGNNV-infected
803 hMMES1 cells and HEK293T cells transfected with Myc empty vector or MmMYL3-Myc
804 with 80,000 magnifications. Bar = 200 nm. (D) HEK293T cells transfected with Myc
805 empty vector or MmMYL3-Myc were infected with RGNNV (MOI = 5) for 24 h, CP (red)
806 and MmMYL3 (green) were detected by immunofluorescence staining. Cell nuclei were
807 stained with DAPI. Bar = 10 μm. Data were collected from three independent experiments

808 and presented as mean ± SD. All results are representative of three similar experiments.

809 **, $P < 0.01$.

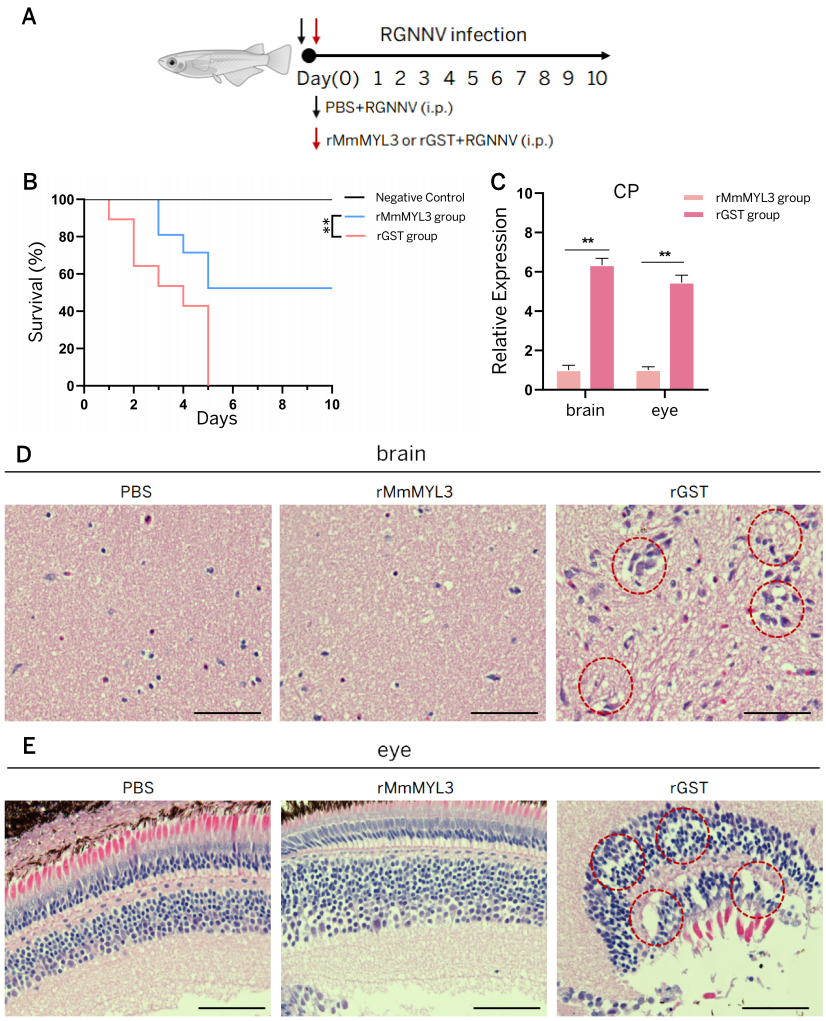

810

811 **Fig. 6. Recombinant MmMYL3 protein treatment protects marine medaka from**

812 **RGNNV pathogenesis.** (A) Schematic representation of the experimental design. RGNNV

813 (100 $TCID_{50}$) was incubated with purified GST-tagged MmMYL3 recombinant protein

814 (rMmMYL3, 500 ng) or GST protein (rGST, 500 ng) for 4 h at 4˚C. Marine medaka were

815 infected with rMmMYL3-RGNNV or GST-RGNNV mixture by intraperitoneal (i.p.)

816 injection, respectively. The negative control group of fishes were injected with the same

817 volume of PBS. (B) Survival rates of marine medaka infected with RGNNV and
818 MmMYL3 or GST protein mixtures. The cumulative survival rate was determined from 1
819 to 10 days post-infection. **, (P<0.01). (C) Quantification of RGNNV CP expression in
820 brain and eye tissues by qRT-PCR. Data are represented as mean ± SD. **, (P < 0.01). (D
821 and E) Histopathological analysis of the eye (D) and brain (E) tissues of fish treated with
822 PBS, rMmMYL3, or rGST. Marine medaka were necropsied and the eyes and brains were
823 collected at day 5 post infection. Hematoxylin and eosin (H&E) staining was used to assess

824 tissue integrity. The vacuolization in eyes and brains were marked by red dotted circle.

825 Bar= 100 μm.

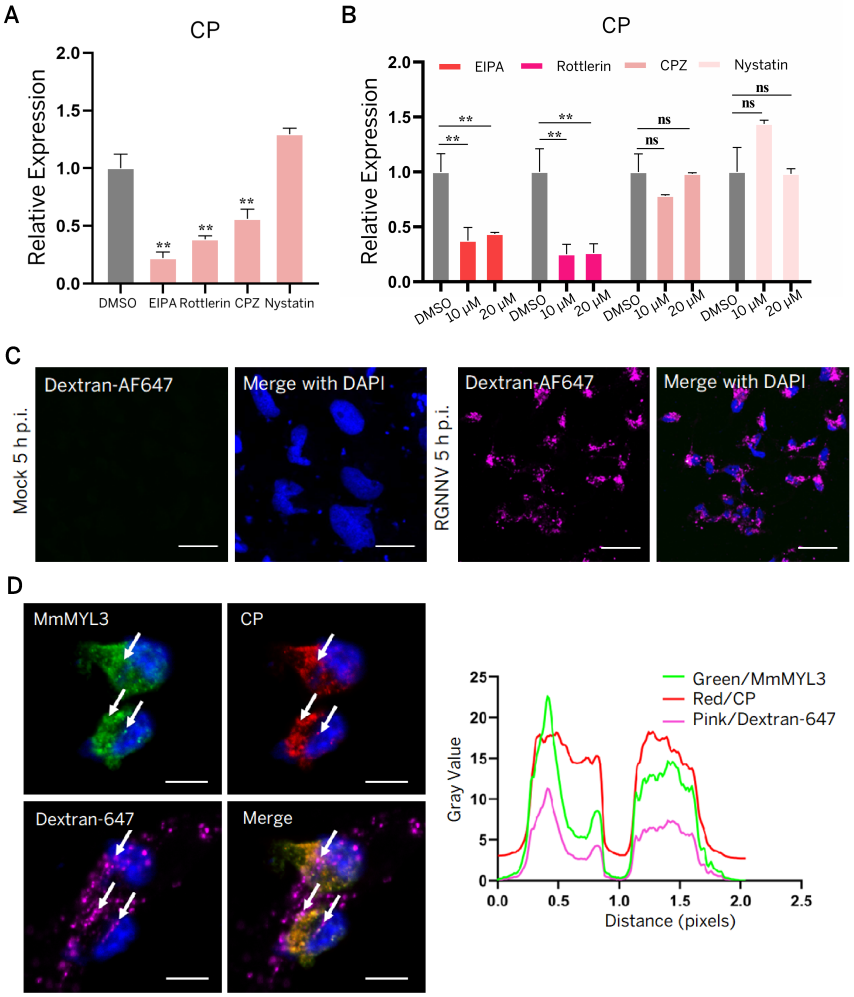

826

827 **Fig. 7. RGNNV triggers macropinocytosis mediated by MmMYL3.** (A) Cells

828 pretreated with EIPA, Rottlerin, CPZ or Nystatin were infected with RGNNV (MOI = 1)

829 for 4 h at 28°C and the expression of CP was analyzed by qRT-PCR. (B) MmMYL3-

830 overexpressing hMMES1 cells were treated with different inhibitors and incubated with

831 RGNNV (MOI = 1) for 4 h at 28°C, the expression of CP was analyzed by qRT-PCR. (C)

832 hMMES1 cells were mock-infected or infected with RGNNV (MOI= 1) in medium

833 containing Alexa Fluor 647-conjugated dextran (10,000 MW). At 4 hpi, cells were fixed

834 and nuclei counterstained with DAPI, and imaged on a confocal microscope. Bar =10 μm.

835 (D) Co-localization of MmMYL3 (green), RGNNV CP (red) and dextran-AF647 in

836 RGNNV-infected hMMES1 cells. Cell nuclei were stained with DAPI. Bar =10 μm. Data

837 were collected from three independent experiments and presented as mean ± SD. All results

838 are representative of three similar experiments. ns, not significant; **, $P < 0.01$.

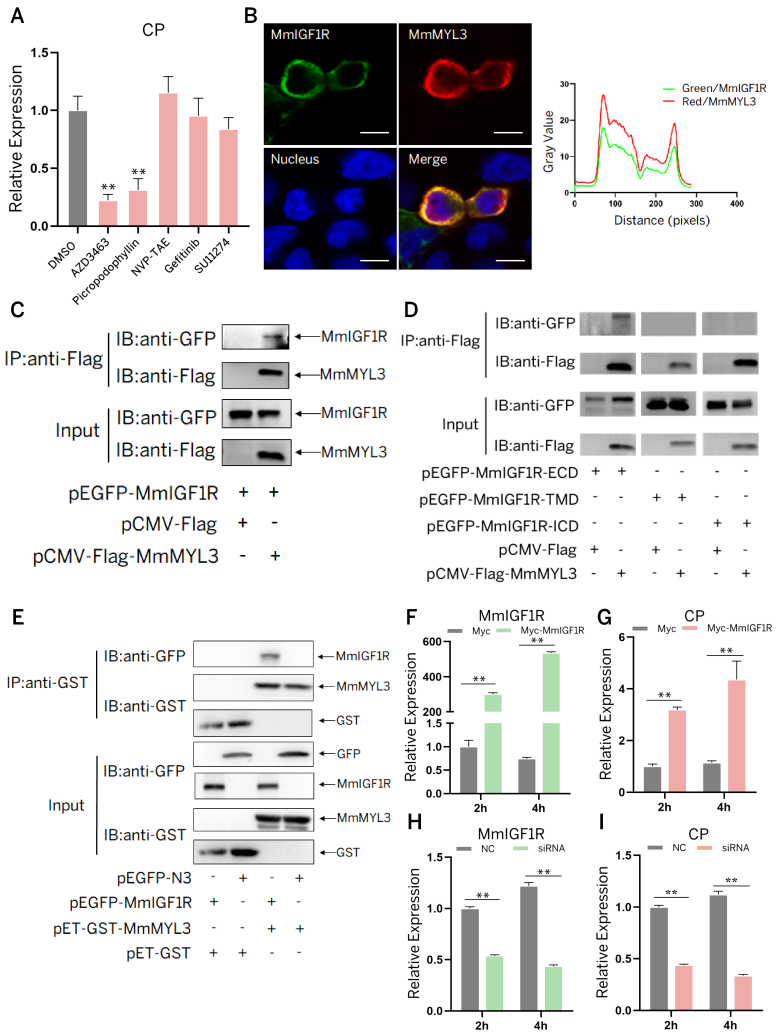

839

840 **Fig. 8. MmIGF1R is involved in MmMYL3 mediated RGNNV internalization.** (A)

841 MmMYL3-overexpressing hMMES1 cells were treated with different RTKs inhibitors,

842 and incubated with RGNNV for 4 h at 28°C, the expression of CP was analyzed by qRT-
843 PCR. (B) MmIGF1R-GFP and MmMYL3-Myc were transfected into HEK293T cells as
844 indicated for immunofluorescence analysis by using anti-Myc (red) abs. Nuclei were
845 stained with DAPI. Bar =10 μm. (C and D) Immunoprecipitation (IP) (with anti-Flag) and
846 immunoblot analysis (with anti-Flag and anti-GFP) of HEK293 cells transfected with
847 plasmids encoding MmMYL3-Flag, MmIGF1R-GFP, MmIGF1R-ECD-GFP, MmIGF1R-
848 TMD-GFP or MmIGF1R-ICD-GFP for 48 h. (E) The lysates of HEK293T cells transfected
849 with indicated plasmids were pulled down with purified MmMYL3-GST or GST proteins.
850 The proteins bound to MmIGF1R and the input were immunoblotted with anti-GST and
851 anti-GFP abs. (F and G) hMMES1 cells were transfected with MmIGF1R-GFP or GFP-N3
852 plasmid (Control) and infected with RGNNV (MOI = 1) for 2 and 4 h respectively. Then,
853 the cells were lysed for qRT-PCR to detect the expression of MmIGF1R and CP. (H and I)
854 qRT-PCR analysis of MmIGF1R and CP mRNA expression of siMmIGF1R- or NC
855 (control)-transfected hMMES1 cells, following infection with RGNNV for 2 and 4 h.Data

856 were collected from three independent experiments and presented as mean ± SD. All results

857 are representative of three similar experiments. **, $P < 0.01$.

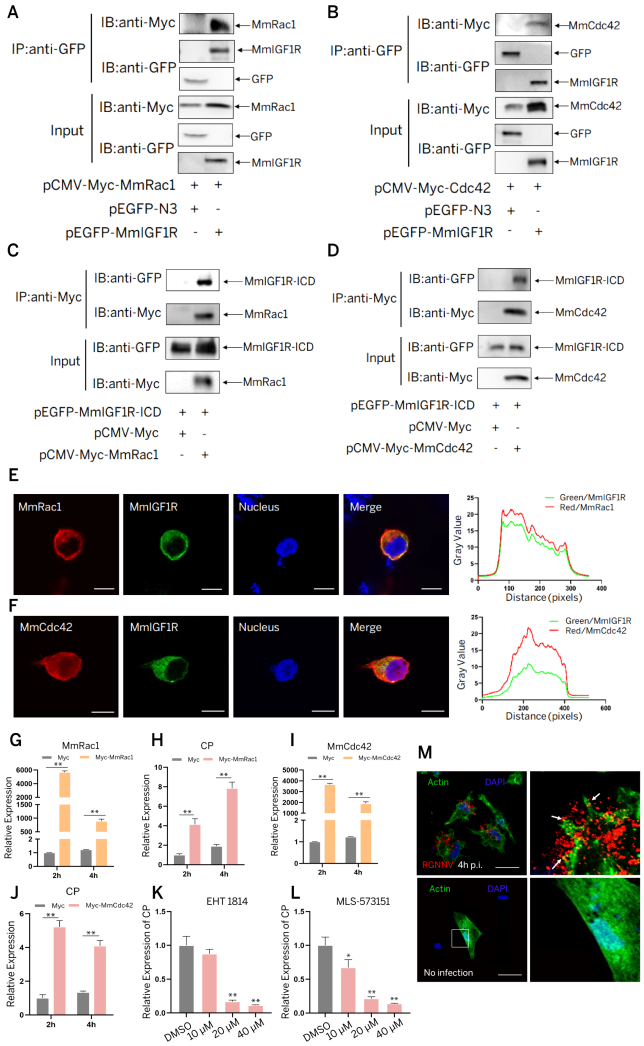

858

859 **Fig. 9. MmRac1 and MmCdc42 regulate RGNNV entry.** (A and B) HEK293T cells

860 were transfected with MmIGF1R-GFP and MmRac1-Myc or MmCdc42-Myc plasmids as

861 indicated for 48 h, and the cell lysates were subjected to coimmunoprecipitation analysis

862 with anti-GFP magnetic beads as described above. (C and D) HEK293T cells were

863 transfected with MmRac1-Myc, MmCdc42-Myc and MmIGF1R-ICD-GFP plasmids,

864 respectively. At 48 h posttransfection, the cell lysates were subjected to

865 coimmunoprecipitation analysis with anti-Myc magnetic beads as indicated. (E and F)
866 MmIGF1R-GFP and MmRac1-Myc or MmCdc42-Myc were transfected into HEK293T
867 cells as indicated for immunofluorescence analysis by using anti-Myc (red) antibodies.
868 Nuclei were stained with DAPI. Bar = 10 μm. (G-J) hMMES1 cells were transfected with
869 MmRac1-Myc, MmCdc42-Myc or pCMV-Myc (Control) plasmids and infected with
870 RGNNV (MOI = 1) for 2 and 4 h respectively. Then, the cells were lysed for qRT-PCR to
871 detect the expression of MmRac1, MmCdc42 and CP. (K and L) hMMES1 cells were
872 treated with inhibitors of Rac1 (EHT1814) or Cdc42 (MLS-573151) for 4 h, then infected
873 with RGNNV (MOI=1) for 4 h at 28°C, the cells were lysed for qRT-PCR to detect the
874 expression of CP. (M) Actin cytoskeleton dynamics are involved in RGNNV entry.
875 hMMES1 cells were exposed to RGNNV (MOI = 1) or PBS for 4 h and actin filaments
876 were labeled with iFluorTM 488 phalloidin (green), then fixed, and permeabilized as
877 described above. Nuclei were stained with DAPI. Images were captured with a 100× oil
878 immersion objective. A higher magnification of the boxed area reveals the formation of
879 actin protrusions at the cell surface membrane (arrows). Bar =10 μm. Data were collected

880 from three independent experiments and presented as mean ± SD. All results are
881 representative of three similar experiments. *, $P < 0.05$; **, $P < 0.01$.

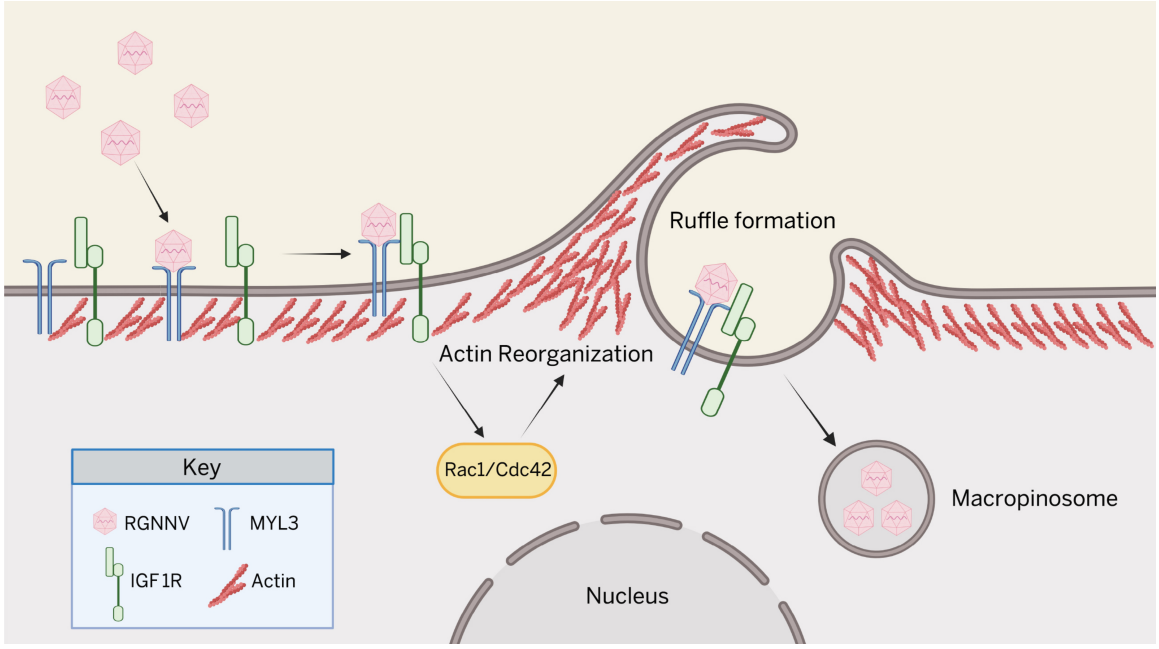

882

883 **Fig. 10. Model of RGNNV entry into host cells via macropinocytosis mediated by**
884 **MmMYL3.** RGNNV particles engage hMMES1 cells through interactions between CP
885 and MYL3, a receptor on the cell surface, which is followed by interactions between MYL3
886 and IGF1R. Then, IGF1R activates and recruits small GTPases Rac1/Cdc42 to induce actin
887 reorganization, facilitate the internalization of RGNNV via macropinocytosis.